

Is cosmic birefringence due to dark energy or dark matter? A tomographic approach

Hiomasa Nakatsuka,¹ Toshiya Namikawa,² and Eiichiro Komatsu^{3,2}

¹*ICRR, University of Tokyo, Kashiwa, 277-8582, Japan*

²*Kavli IPMU (WPI), UTIAS, University of Tokyo, Kashiwa, 277-8583, Japan*

³*Max Planck Institute for Astrophysics, Karl-Schwarzschild-Str. 1, 85748 Garching, Germany*

A pseudoscalar “axionlike” field, ϕ , may explain the 3σ hint of cosmic birefringence observed in the EB power spectrum of the cosmic microwave background (CMB) polarization data. Is ϕ dark energy or dark matter? A tomographic approach can answer this question. The effective mass of dark energy field responsible for the accelerated expansion of the Universe today must be smaller than $m_\phi \simeq 10^{-33}$ eV. If $m_\phi \gtrsim 10^{-32}$ eV, ϕ starts evolving before the epoch of reionization and we should observe different amounts of birefringence from the EB power spectrum at low ($l \lesssim 10$) and high multipoles. Such an observation, which requires a full-sky satellite mission, would rule out ϕ being dark energy. If $m_\phi \gtrsim 10^{-28}$ eV, ϕ starts oscillating during the epoch of recombination, leaving a distinct signature in the EB power spectrum at high multipoles, which can be measured precisely by ground-based CMB observations. Our tomographic approach relies on the shape of the EB power spectrum and is less sensitive to miscalibration of polarization angles.

I. INTRODUCTION

A pseudoscalar “axionlike” field is a candidate for dark matter and dark energy in the Universe [1, 2]. Like pion in the standard model of elementary particles and fields, a pseudoscalar can couple to the electromagnetic tensor $F_{\mu\nu}$ and its Hodge dual $\tilde{F}^{\mu\nu}$ via a Chern-Simons term in the Lagrangian density, $\mathcal{L} \supset -\frac{1}{4}g\phi F_{\mu\nu}\tilde{F}^{\mu\nu}$ [3, 4], where g is the axion-photon coupling constant. This term rotates the plane of linear polarization of photons as they travel through space filled with ϕ [5–7].

Such a rotation produces non-zero odd-parity TB and EB power spectra of the cosmic microwave background (CMB) polarization fields, which vanish in the standard cosmological model [8]. This effect is often referred to as “cosmic birefringence,” as it resembles birefringence in a material (see Ref. [9] for a review).

The plane of linear polarization of CMB photons rotates clockwise on the sky by an angle $\beta = \frac{1}{2}g \int_{t_{\text{LSS}}}^{t_0} dt d\phi/dt$, where $d\phi/dt$ is the total derivative of ϕ along the photon trajectory, and the subscripts “0” and “LSS” denote the present day and the last scattering surface of CMB photons, respectively. The CMB is an ideal target for measuring β , as it is proportional to the path length of photons when ϕ is evolving slowly.

Cosmic birefringence can be caused by ϕ of dark energy [10, 11] and dark matter [12, 13], as well as by possible signatures of quantum gravity [14, 15]. How can we tell the origin? The effective mass of ϕ , $m_\phi^2 \equiv d^2V/d\phi^2$, is the key parameter, where $V(\phi)$ is the potential. The field does not change very much when $m_\phi \lesssim H(t)$, where $H(t)$ is the Hubble expansion rate at a time t ; thus, ϕ would be dark energy today if $m_\phi \lesssim H_0 \equiv H(t_0) \simeq 10^{-33}$ eV. The ϕ field with mass greater than this value would constitute a fraction of dark matter in the Universe today.

A tantalizing hint for β has been found in the EB power spectrum of the *Planck* mission with the statistical significance exceeding 3σ [16–18]. If confirmed with higher statistical significance in future, it would have pro-

found implications for the fundamental physics behind dark energy and dark matter, as well as for quantum gravity. Anticipating such a discovery, in this paper we show how to determine m_ϕ using a tomographic approach to cosmic birefringence.

There are two epochs in which linear polarization of the CMB was generated: (1) the epoch of recombination of hydrogen atoms and the subsequent decoupling of photons from plasma at a redshift of $z_{\text{rec}} \simeq 1090$ [19]; and (2) the epoch of reionization of hydrogen atoms at $z_{\text{rei}} \simeq 7$ [20]. The CMB photons that were last-scattered at these epochs would experience different amounts of cosmic birefringence [21, 22], which changes the relative amplitudes of the EB power spectrum at low ($l \lesssim 10$) and high multipoles. We can use this l dependence to infer β from $z \simeq z_{\text{rec}}$ to z_{rei} and that from $z \simeq z_{\text{rei}}$ to 0, i.e., tomography. For example, if $m_\phi \gtrsim 10^{-31}$ eV, we should not detect the reionization bump in the EB spectrum at $l \lesssim 10$ [23]. Such an observation requires a full-sky satellite mission like *LiteBIRD* [24] and would rule out ϕ being dark energy.

The formula $\beta = \frac{1}{2}g \int_{t_{\text{LSS}}}^{t_0} dt d\phi/dt$ assumes an instantaneous last scattering at t_{LSS} , but a finite duration of last scattering leaves unique signatures in the CMB power spectrum [12]. If $m_\phi \gtrsim 10^{-28}$ eV, ϕ starts oscillating during or earlier than the recombination epoch, modifying the EB power spectrum at high l . This effect can be measured precisely by ground-based CMB observations such as Simons Observatory [25], South Pole Observatory [26], and CMB-S4 [27], which opens up new scientific opportunities for CMB experiments.

In this paper, we solve the Boltzmann equation coupled with the equation of motion (EoM) for ϕ , assuming that ϕ is either a dark energy field or a “spectator” field with negligible energy density. The energy density of ϕ therefore does not enter the Friedmann equation explicitly. We show how the shape of the EB power spectrum depends on m_ϕ , and provide a forecast for future constraints on m_ϕ and $g\phi$.

The tomographic approach can also mitigate partially

the artificial rotation angle, α , by miscalibration of polarization angles of detectors and other instrumental effects [28–32]. The artificial rotation affects the EB power spectrum at all multipoles equally, whereas the tomographic approach relies on the l -dependent effect. For example, the Galactic foreground emission experiences only a negligible amount of birefringence, and we can use the different l dependence of the foreground and CMB power spectra to determine α and β simultaneously [33]. As we show in this paper, the difference between recombination and reionization signals can probe 10^{-32} eV $\lesssim m_\phi \lesssim 10^{-31}$ eV (see Ref. [23] for an earlier, more qualitative study), and details of the shape of the high- l EB power spectrum can probe $m_\phi \gtrsim 10^{-28}$ eV.

The rest of the paper is organized as follows. In Sec. II, we present the Boltzmann equation and the EoM for ϕ [12, 21, 34, 35]. Our approach is different from Ref. [36], which did not solve the EoM. In Sec. III, we solve these equations to calculate the EB power spectrum, and show new features that are important for cosmic birefringence tomography. In Sec. IV, we forecast expected constraints on the axion parameters for experiments similar to *Lite-BIRD* [24], Simons Observatory [25], and CMB-S4 [27]. We discuss possible improvements for our calculation in Sec. V and conclude in Sec. VI.

We use the Friedmann-Lemaître-Robertson-Walker spacetime with a metric tensor given by $a^2(\eta)\text{diag}(-1, \mathbf{1})$, where $a(\eta)$ is the scale factor of the expansion of the Universe. We use the conformal time, η , as time coordinates unless noted otherwise. We focus on the homogeneous axion background, $\phi(\eta)$, and ignore inhomogeneity in ϕ .

II. BOLTZMANN EQUATION FOR ISOTROPIC COSMIC BIREFRINGENCE

A. Setup

We work with the Lagrangian density of axion electrodynamics given by [3, 4]

$$\mathcal{L} = -\frac{1}{2}(\partial_\mu\phi)^2 - V(\phi) - \frac{1}{4}F_{\mu\nu}F^{\mu\nu} - \frac{1}{4}g\phi F_{\mu\nu}\tilde{F}^{\mu\nu}. \quad (1)$$

The dispersion relation of photons is given by $\omega_\pm^2 = k^2(1 \mp g\phi'/k)$, where ω_\pm is the angular frequency of \pm helicity states [5–7]. The $+$ and $-$ states correspond to the right and left circular-polarization modes, respectively, in right-handed coordinates with the z axis taken in the direction of propagation of photons. The prime denotes the derivative with respect to η .

In the WKB limit where ϕ varies slowly so that ω_\pm is much larger than the time evolution of ϕ , i.e., $|\omega'_\pm|/\omega_\pm^2 \ll 1$, the rotation of the plane of linear polarization from η to the present time is written as [5–7]

$$\beta(\eta) \equiv -\int_\eta^{\eta_0} d\eta_1 \frac{\omega_+ - \omega_-}{2} = \frac{g}{2}[\phi(\eta_0) - \phi(\eta)], \quad (2)$$

where η_0 is the conformal time today. Here, we use the CMB convention for the position angle of linear polarization, i.e., $\beta > 0$ is a clockwise rotation in the sky in right-handed coordinates with the z axis taken in the direction of observer's lines of sight. The EoM for ϕ is

$$\phi'' + 2\frac{a'}{a}\phi' + a^2m_\phi^2\phi = 0, \quad (3)$$

for $V(\phi) = m_\phi^2\phi^2/2$.

The field does not evolve very much when $H(\eta) = a'/a^2 \gg m_\phi$. We choose the initial conditions at η_{in} such that $H(\eta_{\text{in}}) \gg m_\phi$, $\phi'(\eta_{\text{in}}) = 0$, and $\phi(\eta_{\text{in}}) = \phi_{\text{in}}$. We do not include the energy density of ϕ in the Friedmann equation explicitly, but use $H(\eta)$ derived from a flat Λ cold dark matter (Λ CDM) model. This approximation is valid when the energy density of ϕ is negligible (e.g., a tiny fraction of dark matter) or the axion mass is so small ($m_\phi \lesssim 10^{-33}$ eV) that it behaves as dark energy. The axion field with a tiny energy fraction can still induce a sizable amount of birefringence [37].

The EoM is a linear equation for ϕ . We therefore introduce a function, $f(\eta) \equiv \phi(\eta)/\phi_{\text{in}}$, which satisfies the same EoM as in Eq. (3) with the initial condition $f(\eta_{\text{in}}) = 1$. The birefringence angle is given by

$$\beta(\eta) = \frac{g\phi_{\text{in}}}{2}[f(\eta_0) - f(\eta)]. \quad (4)$$

B. Boltzmann equation

We work with parity eigenstates of CMB polarization, E and B modes, which have even and odd parity, respectively [38, 39]. In the standard cosmological model, the E and B modes are uncorrelated due to parity symmetry. Cosmic birefringence violates parity symmetry and leads to a correlation between E and B modes [8].

In this paper, we consider only scalar-mode perturbations and ignore tensor modes. The evolution of linear polarization of CMB photons follows the Boltzmann equation [19]. We expand Stokes parameters of linear polarization, Q and U , in Fourier space with the wave vector \mathbf{q} . We define the cosine between \mathbf{q} and the photon propagation direction as $\mu \equiv \mathbf{q} \cdot \mathbf{k}/(qk)$. We then write the Boltzmann equation for the Fourier coefficients of $Q \pm iU$, ${}_{\pm 2}\Delta_P(\eta, q, \mu)$, as [9]

$$\begin{aligned} {}_{\pm 2}\Delta'_P + iq\mu {}_{\pm 2}\Delta_P &= \tau' \left[-{}_{\pm 2}\Delta_P + \sqrt{\frac{6\pi}{5}} {}_{\pm 2}Y_l^0(\mu)\Pi \right] \\ &\pm 2i\beta' {}_{\pm 2}\Delta_P, \end{aligned} \quad (5)$$

where ${}_{\pm 2}Y_l^m$ is the spin-2 spherical harmonics, $\Pi(\eta, q)$ is the polarization source term [38], $\beta' \equiv g\phi'/2$ gives $\beta(\eta) = \int_\eta^{\eta_0} d\eta_1 \beta'(\eta_1)$ in Eq. (2), and $\tau' \equiv a(\eta)n_e(\eta)\sigma_T$ is the differential optical depth with the Thomson scattering cross section σ_T and the number density of electrons n_e .

With the μ dependence of $\pm_2\Delta_P$ expanded in spin-2 spherical harmonics,

$$\pm_2\Delta_P(\eta, q, \mu) = \sum_l i^{-l} \sqrt{4\pi(2l+1)} \pm_2\Delta_{P,l}(\eta, q) \pm_2Y_l^0(\mu), \quad (6)$$

the formal solution for the Boltzmann equation is [21]

$$\pm_2\Delta_{P,l}(\eta_0, q) = -\frac{3}{4} \sqrt{\frac{(l+2)!}{(l-2)!}} \int_0^{\eta_0} d\eta \tau' e^{-\tau(\eta)} \Pi \frac{j_l(x)}{x^2} \times \exp[\pm 2i\beta(\eta)], \quad (7)$$

where $j_l(x)$ is the spherical Bessel function with $x = q(\eta_0 - \eta)$ and $\tau(\eta) = \int_\eta^{\eta_0} d\eta_1 \tau'(\eta_1)$.

Cosmic birefringence induces an imaginary part of $\pm_2\Delta_{P,l}(\eta_0, q)$, which leads to B modes. We write the coefficients of E and B modes as [38]

$$\Delta_{E,l}(q) \pm i\Delta_{B,l}(q) \equiv \pm_2\Delta_{P,l}(\eta_0, q). \quad (8)$$

Using Eqs. (7) and (8), the CMB polarization power spectrum is given by

$$C_l^{XY} = 4\pi \int d(\ln q) \mathcal{P}_s(q) \Delta_{X,l}(q) \Delta_{Y,l}(q), \quad (9)$$

where $\mathcal{P}_s(q)$ is the primordial scalar curvature power spectrum and $X, Y = E$ or B . While cosmic birefringence modifies all polarization modes, we focus on the EB power spectrum since it is more sensitive than TB for the current and future generations of CMB experiments with low polarization noise.

We implement Eq. (7) in the CLASS code [40, 41] and calculate C_l^{EB} with the best-fitting *Planck* 2018 cosmological parameters for a flat Λ CDM model [42]. One significant change made to the code is the treatment of B modes induced by scalar perturbations. Cosmic birefringence transfers a part of scalar E modes into B modes, and we need to compute $\Delta_{B,l}$ which vanishes otherwise.

C. Axion mass and the visibility function

Cosmic birefringence tomography relies on two epochs in which CMB polarization was generated. In Fig. 1, we show the visibility function, the probability density of photons being last scattered, defined by $g_{\text{vis}}(\eta) \equiv \sigma_{TA}(\eta)n_e(\eta)e^{-\tau(\eta)}$, as a function of redshift with the thermal history obtained from the RECFAST code [43–45]. As expected, the visibility function has the largest value at the recombination and photon decoupling epoch, $z_{\text{rec}} \simeq 1090$. The second peak appears at $z_{\text{rei}} \simeq 7$.

In Fig. 2, we compare the evolution of ϕ with the epochs of recombination and reionization. The axion with $m_\phi = 10^{-28.0}$ eV (green line) starts evolving significantly before recombination, which experiences a reduction in the amount of birefringence [12, 13].

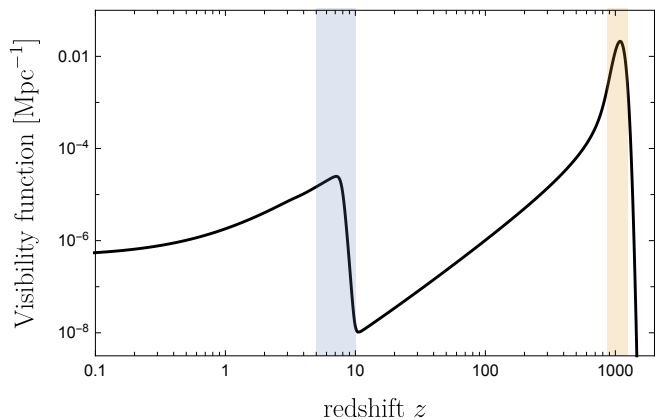


FIG. 1. The visibility function as a function of redshift z . The orange and blue regions show the recombination and reionization epochs, respectively. The reionization is included using the \tanh model with $z_{\text{rei}} = 7.82$ [42, 46].

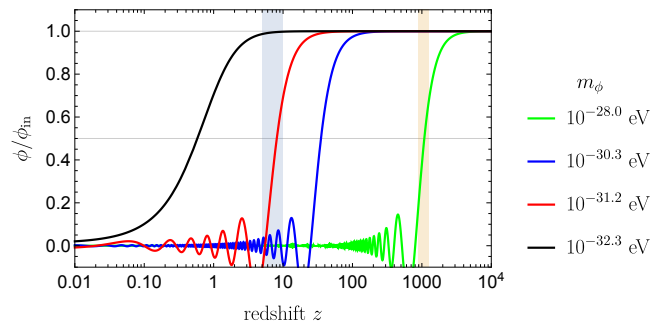


FIG. 2. Evolution of ϕ for $m_\phi = 10^{-28.0}$ (green), $10^{-30.3}$ (blue), $10^{-31.2}$ (red), and $10^{-32.3}$ eV (black). The shaded regions show recombination and reionization epochs as in Fig. 1.

The axion with $m_\phi = 10^{-30.3}$ eV (blue line) starts evolving after recombination but has decayed before reionization; thus, very little cosmic birefringence would occur after reionization. The axion with $m_\phi = 10^{-31.2}$ eV (red line) starts oscillating during reionization, and that with $m_\phi = 10^{-32.3}$ eV (black line) evolves only after reionization. The amplitude of the reionization bump in C_l^{EB} is therefore sensitive to 10^{-32} eV $\lesssim m_\phi \lesssim 10^{-31}$ eV.

For $m_\phi \lesssim 10^{-32}$ eV we expect C_l^{EB} to be scaled by a single β at all l . The polarization modes [Eq. (8)] are simply given by $\Delta_{E,l} \pm i\Delta_{B,l} = e^{\pm 2i\beta}(\tilde{\Delta}_{E,l} \pm i\tilde{\Delta}_{B,l})$, where the tildes denote the values before cosmic birefringence. Then, the polarization power spectra after birefringence are given by [21, 47]

$$C_l^{EE} = \cos^2(2\beta)\tilde{C}_l^{EE} + \sin^2(2\beta)\tilde{C}_l^{BB}, \quad (10)$$

$$C_l^{BB} = \cos^2(2\beta)\tilde{C}_l^{BB} + \sin^2(2\beta)\tilde{C}_l^{EE}, \quad (11)$$

$$C_l^{EB} = \frac{1}{2} \sin(4\beta)(\tilde{C}_l^{EE} - \tilde{C}_l^{BB}). \quad (12)$$

In this case, $C_l^{EB} \propto C_l^{EE}$ when we ignore the primordial B modes, and β is degenerate with the instrumental mis-

calibration angle α [29, 30]. The tomography approach breaks this degeneracy by using the change in *shape* of C_l^{EB} induced by either $m_\phi \gtrsim 10^{-32}$ eV [23] or the Galactic foreground [33].

III. COSMIC BIREFRINGENCE FROM RECOMBINATION AND REIONIZATION

A. Toy example

To build an intuitive understanding of the full numerical result for C_l^{EB} due to evolving ϕ , we first study a toy example in which $\beta(z)$ integrated from z to the present time [Eq. (2)] changes abruptly:

$$\beta(z) = \begin{cases} 0 & \text{for } z = 0 \\ \beta_{\text{rei}} & \text{for } 0 < z \leq 10, \\ \beta_{\text{rec}} & \text{for } 10 < z \end{cases} \quad (13)$$

where β_{rei} and β_{rec} are piecewise constant angles integrated out to $z = 10$ and recombination, respectively.

In the top panel of Fig. 3 we show C_l^{EB} for $\{\beta_{\text{rei}}[\text{deg}], \beta_{\text{rec}}[\text{deg}]\} = \{1, 1\}$ (red), $\{0.5, 1\}$ (green), and $\{0, 1\}$ (blue). All lines coincide at $l \gtrsim 20$ because β_{rec} is the same. As β_{rei} decreases, the reionization bump of C_l^{EB} also decreases. However, the reionization bump does not disappear even for $\beta_{\text{rei}} = 0$.

The shape of C_l^{EB} can be understood as follows. The E and B modes are written as

$$\Delta_{E,l} \pm i\Delta_{B,l} = \sum_{x=\text{rei}, \text{rec}} e^{\pm 2i\beta_x} (\tilde{\Delta}_{E,l}^{(x)} \pm i\tilde{\Delta}_{B,l}^{(x)}). \quad (14)$$

Ignoring the primordial B modes, C_l^{EB} is given by

$$C_l^{EB} = \frac{1}{2} \sin(4\beta_{\text{rec}}) \tilde{C}_l^{E\text{rec}, E\text{rec}} + \frac{1}{2} \sin(4\beta_{\text{rei}}) \tilde{C}_l^{E\text{rei}, E\text{rei}} + \sin[2(\beta_{\text{rei}} + \beta_{\text{rec}})] \tilde{C}_l^{E\text{rei}, E\text{rec}}, \quad (15)$$

where $\tilde{C}_l^{Ex, Ey}$ is the cross power spectrum of $\tilde{\Delta}_{E,l}^{(x)}$ and $\tilde{\Delta}_{E,l}^{(y)}$ with $x, y = \text{rei}, \text{rec}$. The first term dominates at $l \gtrsim 20$. The second term produces the reionization bump at $l \lesssim 10$. The third term was overlooked in Ref. [23]. The cross correlation of reionization and recombination E modes induces a small reionization bump even when the rotation angle is zero at reionization. This effect appears in the blue line of Fig. 3 where a small bump is seen at $l \lesssim 10$. Therefore, there is always some C_l^{EB} at low l .

When the rotation angle depends on time, C_l^{EB} is no longer given by Eq. (12). We thus define an effective angle at each l as

$$\beta_l^{(\text{eff})} \equiv \frac{1}{4} \arcsin\left(\frac{2x_l}{1+x_l^2}\right) \quad \text{with } x_l = \frac{C_l^{EB}}{C_l^{EE}}, \quad (16)$$

which is defined so as to reproduce Eq. (12) for the simplest case. Note that $\beta_l^{(\text{eff})} \simeq C_l^{EB}/(2C_l^{EE})$ for

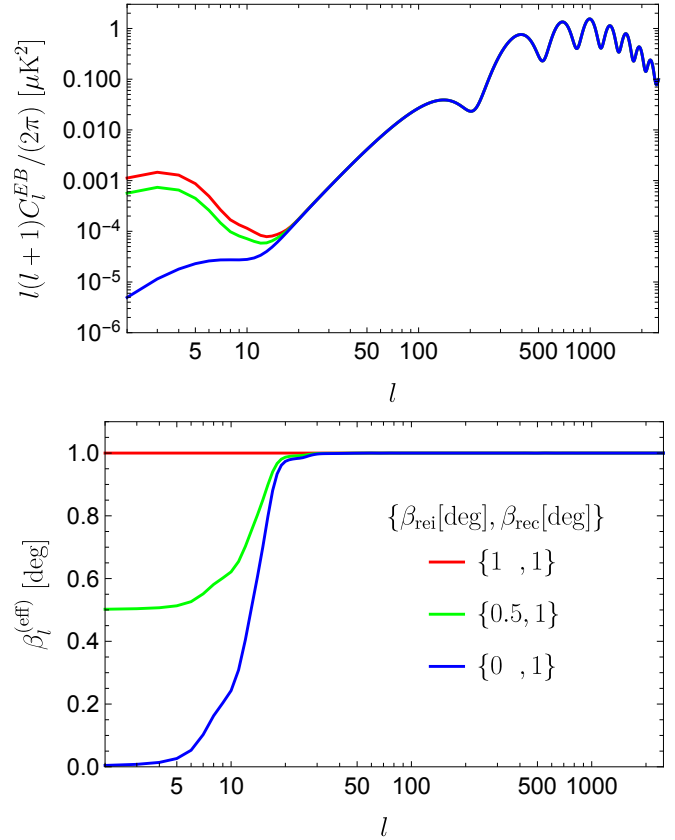


FIG. 3. The EB power spectrum from piecewise constant angles given in Eq. (13): $\beta = \beta_{\text{rec}}$ for $z > 10$ and $\beta = \beta_{\text{rei}}$ for $z \leq 10$. The top and bottom panels show $l(l+1)C_l^{EB}/(2\pi)$ and the effective angles given in Eq. (16), respectively.

$C_l^{EB}/C_l^{EE} \ll 1$. In the bottom panel of Fig. 3, we show effective angles for the piecewise constant angles given in Eq. (13). The effective angle reproduces $\beta_l^{(\text{eff})} = \beta_{\text{rec}}$ for $l \gg 20$, where the recombination contribution dominates. It converges to β_{rei} for $l \ll 20$, where the reionization contribution dominates.

B. EB power spectrum from axion dynamics

In the left panel of Fig. 4 we present the full Boltzmann solution for C_l^{EB} with axion dynamics shown in Fig. 2. In the right panel we show the corresponding $\beta_l^{(\text{eff})}$. We use $g\phi_{\text{in}}/2 = -1 \text{ deg} \simeq -0.01745$, which determines the overall amplitude of β via Eq. (4).

1. Reionization bump as a probe of $m_\phi \lesssim 10^{-31}$ eV

We first study $m_\phi \lesssim 10^{-30}$ eV. As ϕ starts evolving well after the recombination epoch, the only difference appears in the reionization bump. We find the largest amplitude for $m_\phi \simeq 10^{-32}$ eV, for which ϕ starts evolving

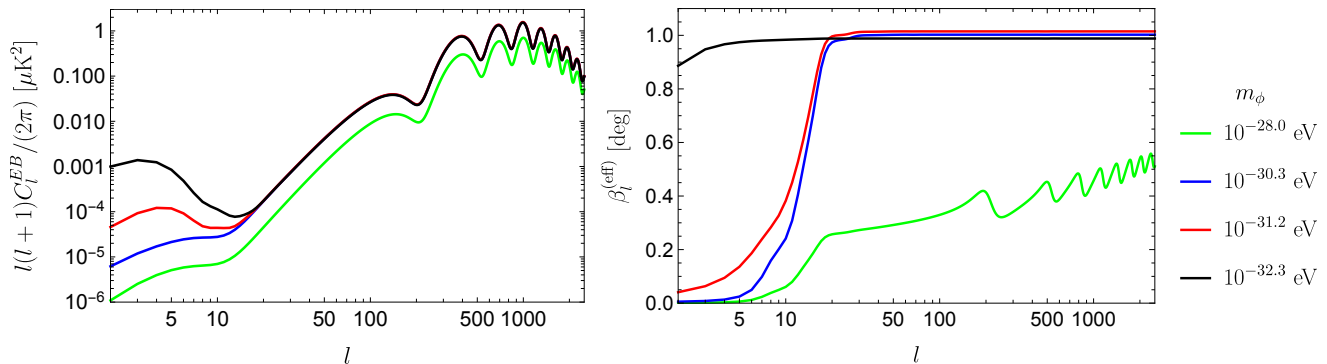


FIG. 4. Same as Fig. 3, but for axion dynamics shown in Fig. 2.

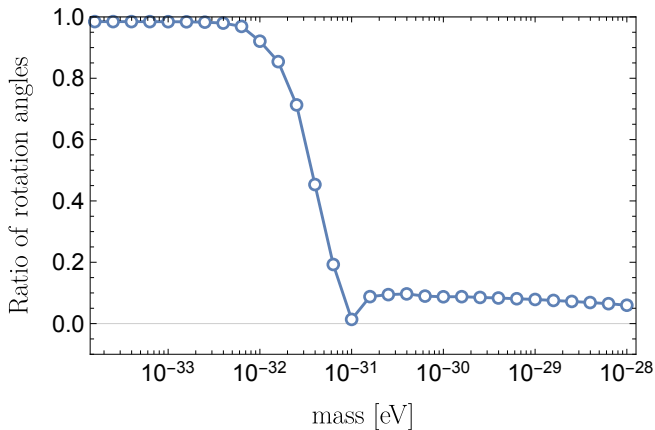


FIG. 5. Ratio of the effective cosmic birefringence angles from reionization and recombination defined in Eq. (17). The ratio is sensitive to the change in the axion mass over 10^{-32} eV $\lesssim m_\phi \lesssim 10^{-31}$ eV.

only after reionization. The amplitude decreases as m_ϕ increases; however, the reionization bump does not disappear even for $m_\phi = 10^{-30.3}$ eV, as explained in Sec. III A. We can therefore probe m_ϕ that falls between the black and blue lines in the left panel of Fig. 4.

To make this statement more quantitative, we define the ratio of the effective angles for low and high l as

$$\frac{\sum_{l=2}^{10} \beta_l^{(\text{eff})}/9}{\sum_{l=11}^{500} \beta_l^{(\text{eff})}/490}. \quad (17)$$

In Fig. 5 we find that the ratio is sensitive to the change in mass over 10^{-32} eV $\lesssim m_\phi \lesssim 10^{-31}$ eV. We thus conclude that this is the range of m_ϕ we can probe using the relative amplitudes of the reionization bump and the high- l EB power spectrum.

2. High- l features as a probe of $m_\phi \gtrsim 10^{-28}$ eV

The axion starts oscillating during recombination for $m_\phi \gtrsim 10^{-28}$ eV. Photons last-scattered at different times

experience different amounts of rotation of the plane of linear polarization, which can lead to partial cancellation of cosmic birefringence [12, 13, 48] as well as to complex features in C_l^{EB} at high l that can be used to probe $m_\phi \gtrsim 10^{-28}$ eV in a completely new way.

In the left panel of Fig. 6 we show C_l^{EB} for axion dynamics shown in the right panel. There are two effects on C_l^{EB} : the overall amplitude and shape.

We first discuss the amplitude, which changes dramatically depending on the value of ϕ during recombination. For $m_\phi = 10^{-28.8}$ eV, ϕ is nearly constant, which results in $C_l^{EB} \propto C_l^{EE}$ except for the reionization bump. For $m_\phi = 10^{-27.9}$ eV, ϕ starts evolving during recombination, resulting in a smaller C_l^{EB} . For $m_\phi = 10^{-27.8}$ eV, ϕ averaged over recombination is tiny, resulting in a highly suppressed C_l^{EB} . For $m_\phi = 10^{-27.7}$ eV, ϕ averaged over recombination is *negative*, hence $C_l^{EB} < 0$.

In the previous work that did not solve the Boltzmann equation, the amplitude of C_l^{EB} has been calculated by averaging ϕ over the visibility function [13, 37, 48]:

$$\langle \beta \rangle \equiv \frac{g}{2} [\phi(\eta_0) - \langle \phi \rangle_{\text{LSS}}], \quad (18)$$

where

$$\langle \phi \rangle_{\text{LSS}} \equiv \frac{\int_0^{\eta_{z=10}} d\eta g_{\text{vis}}(\eta) \phi(\eta)}{\int_0^{\eta_{z=10}} d\eta g_{\text{vis}}(\eta)}, \quad (19)$$

with $\eta_{z=10}$ being a conformal time at $z = 10$. Since we focus on the rotation angle from recombination, the average is limited to $z > 10$ with $\int_0^{\eta_{z=10}} d\eta g_{\text{vis}}(\eta) \simeq 0.95$. We use $g_{\text{vis}}(\eta)$ computed with CLASS as shown in Fig. 1.

In Fig. 7 we compare $\beta_l^{(\text{eff})}$ computed from the Boltzmann equation and Eq. (18) for $m_\phi = 10^{-27.9}$ eV (top panel) and $m_\phi = 10^{-27.8}$ eV (bottom). It is clear that $\beta_l^{(\text{eff})}$ shows much more complex features than just the average value $\langle \beta \rangle$ shown by the horizontal lines.

How can we understand such complex dependence of $\beta_l^{(\text{eff})}$ (hence C_l^{EB}) on m_ϕ ? We find that the location of the acoustic peaks in C_l^{EB} for $m_\phi = 10^{-27.9}$ eV shifts to higher l compared to that for $m_\phi = 10^{-28.8}$ eV (see

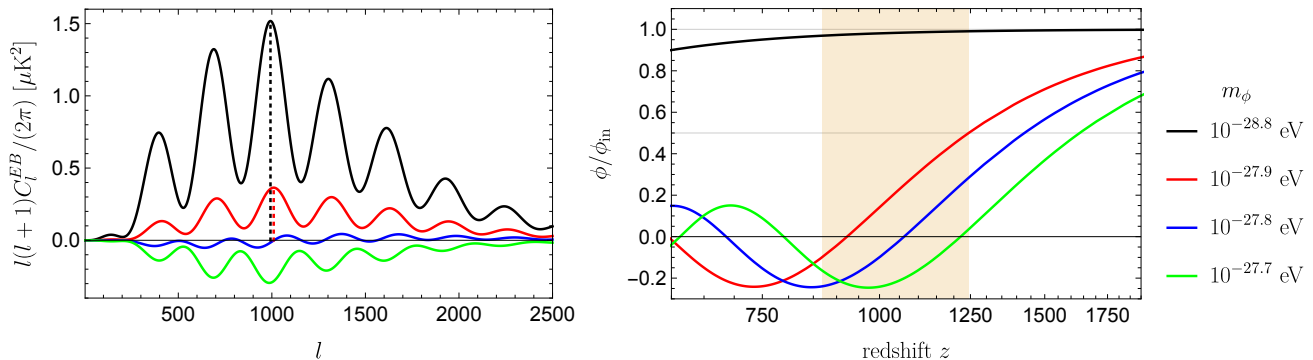


FIG. 6. The EB power spectrum for large m_ϕ . The left panel shows $l(l+1)C_l^{EB}/(2\pi)$ for $m_\phi = 10^{-28.8}$ (black), $10^{-27.9}$ (red), $10^{-27.8}$ (blue), and $10^{-27.7}$ eV (green). The dotted vertical lines show the positions of the third peak. The right panel shows axion dynamics for each m_ϕ . The shaded region shows the recombination epoch as in Fig. 1.

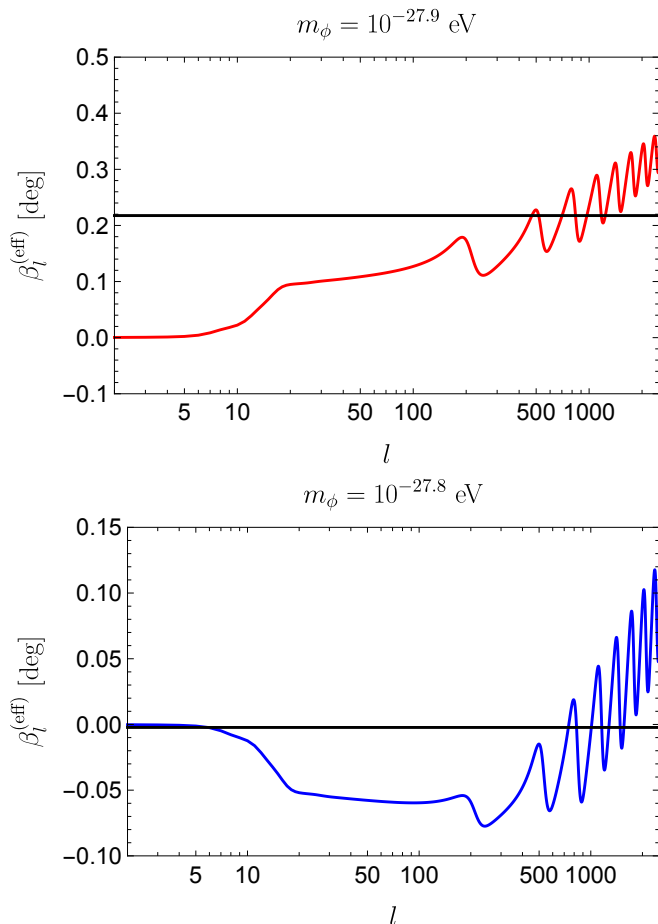


FIG. 7. The effective rotation angles from the Boltzmann equation (wiggly lines) and $\langle\beta\rangle$ given in Eq. (18) (horizontal lines) for $m_\phi = 10^{-27.9}$ eV (top) and $10^{-27.8}$ eV (bottom).

the vertical dotted lines in Fig. 6). This peak shift is the origin of the oscillating behavior of $\beta_l^{(\text{eff})}$ at $l > 100$.

The peak location is determined by D_A/r_s , where r_s and D_A are the sound horizon and angular diameter dis-

tance at last scattering, respectively. In our fiducial cosmological model, $D_A/r_s \simeq (1+z_{\text{LSS}})^{1/2}$ where z_{LSS} is the redshift of last scattering. For $m_\phi = 10^{-27.9}$ eV, ϕ starts evolving before recombination, and the B modes are mainly generated in the early stage of recombination. In such case, D_A/r_s for the induced B modes becomes effectively large and the peaks shift to higher l . If $m_\phi = 10^{-27.7}$ eV, the time when polarization is mostly produced is close to that for $m_\phi = 10^{-28.8}$ eV and the peak locations are almost identical to those of the black line while the amplitude is negative.

These features are important: we can use this complex dependence of C_l^{EB} to determine m_ϕ in a completely new manner. While the overall amplitude $\langle\beta\rangle$ is degenerate with the miscalibration angle α (unless we have access to $l \lesssim 10$), the l dependence is not. This is relevant for ground-based CMB experiments (Sec. IV B).

IV. FORECAST

A. Simultaneous determination of α and cosmic birefringence with the reionization signal

We first consider the case in which we simultaneously constrain cosmic birefringence and miscalibration angles, α , using the reionization bump in C_l^{EB} [23]. As explained in Sec. III B 1, the axion with $m_\phi \gtrsim 10^{-32}$ eV changes relative amplitudes of C_l^{EB} at low and high l , which cannot be mimicked fully by α because it affects all multipoles equally via Eq. (12) with $\beta \rightarrow \alpha$.

In Ref. [23], C_l^{EB} was modeled as the sum of the reionization and recombination contributions:

$$C_l^{EB} = \sum_{x=\text{rei,rec}} 2\beta_x (C_l^{EE,x,\text{lens}} - C_l^{BB,x,\text{lens}}), \quad (20)$$

where $C_l^{EE,x,\text{lens}}$ and $C_l^{BB,x,\text{lens}}$ are the lensed E - and B -mode power spectra, respectively. As shown in Eq. (15), however, we cannot decompose C_l^{EB} in this way. Therefore, we constrain the axion parameters instead of β_x .

Assuming that the observed E - and B modes obey a multivariate Gaussian distribution with zero mean, the Fisher information matrix is given by [49]

$$\mathbf{F}_{ij} = f_{\text{sky}} \sum_{l=2}^{l_{\text{max}}} \frac{2l+1}{2} \text{Tr} \left(\mathbf{C}_l^{-1} \frac{\partial \mathbf{C}_l}{\partial p_i} \mathbf{C}_l^{-1} \frac{\partial \mathbf{C}_l}{\partial p_j} \right) \Big|_{p_i=p_{i,\text{fid}}}, \quad (21)$$

where l_{max} is the maximum multipole included in the analysis, f_{sky} is a sky fraction used for the analysis, p_i are the parameters to be constrained, $p_{i,\text{fid}}$ are the fiducial parameter values, and the covariance matrix of the observed E - and B modes is given by

$$\mathbf{C}_l \equiv \begin{pmatrix} \hat{C}_l^{EE} & \hat{C}_l^{EB} \\ \hat{C}_l^{EB} & \hat{C}_l^{BB} \end{pmatrix}. \quad (22)$$

The covariance matrix contains the total power spectra, \hat{C}^{EE} , \hat{C}^{EB} and \hat{C}^{BB} , including the lensed CMB, noise, and Galactic foregrounds after component separation. The 1σ constraint on p_i is given by $\sigma(p_i) = (\{\mathbf{F}^{-1}\}_{ii})^{1/2}$.

We consider two parameters, $p_1 \equiv g\phi_{\text{in}}/2$ and $p_2 \equiv \alpha$, and set their fiducial values to be $p_{i,\text{fid}} \equiv 0$. As the E - and B -mode spectra do not have a linear term of p_i and their derivatives with respect to p_i at $p_{i,\text{fid}} = 0$ vanish, $\partial \mathbf{C}_l / \partial p_i|_{p_i=0}$ contains only off-diagonal elements, $\partial C_l^{EB} / \partial p_i|_{p_i=0}$. The Fisher matrix simplifies to [23]

$$\mathbf{F}_{ij} = f_{\text{sky}} \sum_{l=2}^{l_{\text{max}}} \frac{2l+1}{\hat{C}_l^{EE} \hat{C}_l^{BB}} \frac{\partial \hat{C}_l^{EB}}{\partial p_i} \frac{\partial \hat{C}_l^{EB}}{\partial p_j} \Big|_{p_i=0}. \quad (23)$$

We assume a *LiteBIRD*-like white noise ($2\mu\text{K}\cdot\text{arcmin}$), angular resolution (30 arcmin), $f_{\text{sky}} = 0.7$, and the residual Galactic foregrounds obtained by Ref. [50]. We set $l_{\text{max}} = 500$ because of the angular resolution.

The impact of gravitational lensing on C_l^{EB} would be negligible in the Fisher matrix. Lensing does not create C_l^{EB} but only distorts small-scale polarization anisotropies. To see this, we first note that C_l^{EB} is approximately given by Eq. (15). As discussed in Ref. [51], the two operators, lensing and birefringence, commute, and lensing replaces C_l^{EE} in Eq. (15) with $C_l^{EE,\text{lens}} - C_l^{BB,\text{lens}}$. As $C_l^{BB,\text{lens}} \ll C_l^{EE,\text{lens}}$ at $l \ll 5000$ and C_l^{EE} is modified by lensing only at high l , we ignore the gravitational lensing effect on C_l^{EB} .

Fig. 8 shows the expected error contours in the two-dimensional parameter space, $g\phi_{\text{in}}/2$ and α , for a given m_ϕ . For $m_\phi = 10^{-32}\text{ eV}$ the reionization bump in C_l^{EB} is close to its maximum amplitude as explained in Sec. III B 1. In this case C_l^{EB} becomes close to that of the miscalibration angle, and $g\phi_{\text{in}}/2$ and α are strongly degenerate. For $m_\phi = 10^{-30}\text{ eV}$ the reionization bump is suppressed and the degeneracy is reduced. We thus confirm and make more precise the result of Ref. [23].

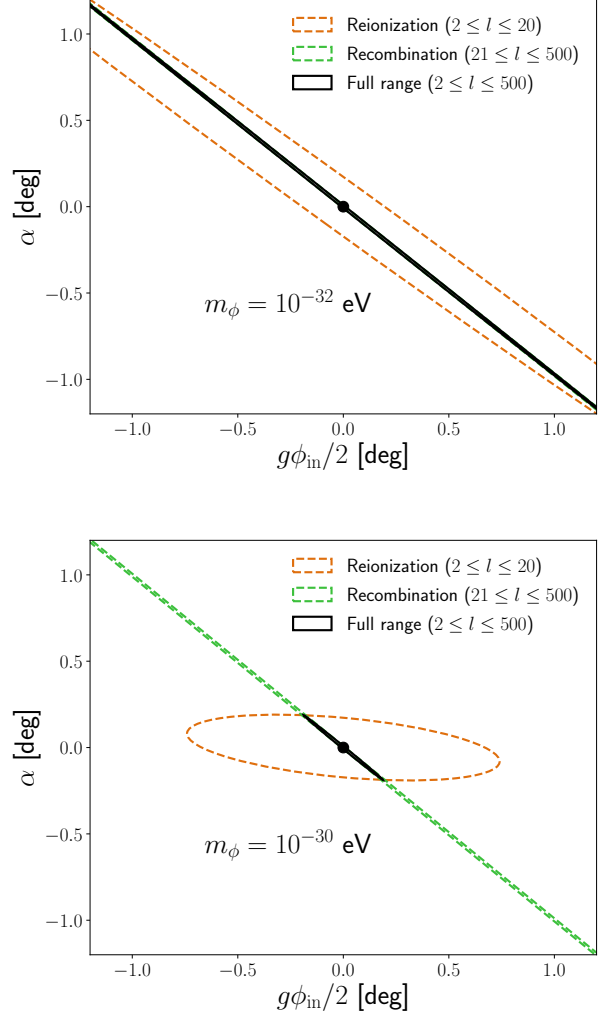


FIG. 8. The expected 1σ error contours in the two-dimensional parameter space (α and $g\phi_{\text{in}}/2$ in units of degrees). The axion masses are $m_\phi = 10^{-32}\text{ eV}$ (top) and 10^{-30} eV (bottom). We show the results from the full l range (black), reionization bump ($2 \leq l \leq 20$; orange dashed), and high multipoles ($21 \leq l \leq 500$; green dot-dashed). We assume a *LiteBIRD*-like experiment without delensing.

B. Constraining the axion mass

Next, we consider joint constraints on m_ϕ , $g\phi_{\text{in}}/2$, and α . Since C_l^{EB} depends on m_ϕ nonlinearly, the Fisher matrix formalism, in which the errors are estimated from curvature of the posterior distribution around the fiducial value, does not provide accurate results. We thus use the likelihood analysis. We define χ^2 as

$$\chi^2(\mathbf{p}) = f_{\text{sky}} \sum_{l=l_{\text{min}}}^{l_{\text{max}}} (2l+1) \frac{[\hat{C}_l^{EB} - C_l^{EB,\text{th}}(\mathbf{p})]^2}{\hat{C}_l^{EE} \hat{C}_l^{BB}}, \quad (24)$$

where $C_l^{EB,th}$ is a theoretical model for the EB power spectrum and is given as the sum of the contributions from cosmic birefringence and α . For a given observed \widehat{C}_l^{EB} we compute χ^2 for each parameter set, $\mathbf{p} = (m_\phi, g\phi_{in}/2, \alpha)$, and obtain the posterior distribution, $P(\mathbf{p}|\widehat{C}^{EB}) \propto \exp[-\chi^2(\mathbf{p})/2]$.

We consider specifications similar to *LiteBIRD* [24], Simons Observatory (SO; [25]), and CMB-S4 [27]. For SO we assume $l_{min} = 100$, $l_{max} = 2500$, $6\mu\text{K-arcmin}$ white noise, 1 arcmin Gaussian beam, $f_{sky} = 0.4$, and no foregrounds. We also assume 30% residual lensing-induced B modes after delensing [52]. For CMB-S4 we assume the same beam, l_{min} , l_{max} , and f_{sky} , but with $1\mu\text{K-arcmin}$ noise and 10% residual lensed B modes [53].

Fig. 9 shows the expected 1 and 2 σ contours on $\log_{10} m_\phi$ and $g\phi_{in}/2$. We consider the *LiteBIRD*-like experiment with specifications given in Sec. IV A. The fiducial axion mass is $m_{\phi, fid} = 10^{-30}$ eV and $g\phi_{in}/2$ is obtained from $\beta_{rec} = 0.35$ deg [16–18] via Eq. (18). The fiducial value of α is set to zero. We marginalize the posterior distribution over α using a prior distribution obtained from calibration of instruments. Specifically, we use a Gaussian prior, $\exp[-\alpha^2/(2\sigma_\alpha^2)]$, with $\sigma_\alpha = 0.5$ deg (top) and 0.1 deg (bottom). The former precision is achieved already for calibration of the current generation of CMB experiments [54–56], whereas the latter can be achieved by employing new calibration strategy [57–60].

The black dashed lines show the values of $|g\phi_{in}/2|$ giving $\beta_{rec} = 0.35$ deg for each m_ϕ . The spikes in $m_\phi > 10^{-28}$ eV occur when C_l^{EB} at high l becomes highly suppressed (see the blue line in Fig. 6). That is to say, we need a larger value of $|g\phi_{in}/2|$ to compensate for suppression of C_l^{EB} by a small value of $\langle\phi\rangle_{LSS}$ [Eq. (19)].

We find that the prior on α tightens the constraint on the overall amplitude parameter ($g\phi_{in}$) significantly, but m_ϕ can be constrained almost independently of the prior. We also find the same trend when removing the prior on α entirely. This is because the information on m_ϕ comes from the shape of C_l^{EB} . For $m_{\phi, fid} = 10^{-30}$ eV the reionization bump is already at its minimum (see the blue line in Fig. 4). Therefore, the shape of C_l^{EB} can tell us that m_ϕ is greater than 10^{-32} eV, but cannot tell how large it is until m_ϕ is so large that it affects the shape at high l . This explains an upper bound, $m_\phi \lesssim 10^{-28}$ eV.

The “islands” of parameter space seen in $m_\phi > 10^{-28}$ eV are allowed because the peak locations of C_l^{EB} for the respective m_ϕ in the islands happen to coincide with those for the fiducial mass of 10^{-30} eV, while the amplitudes are adjusted by varying $g\phi_{in}$. The islands shrink when $g\phi_{in}$ is constrained by a tighter prior on α .

For $m_{\phi, fid} = 10^{-28}$ eV the shape of C_l^{EB} at high l becomes quite different from that of α , which enables us to determine m_ϕ . However, the *LiteBIRD*-like experiment cannot determine such a large m_ϕ accurately because of the limited angular resolution, giving only discrete islands of constraints (Fig. 10). Therefore, it gives effectively a lower bound for m_ϕ almost independently of σ_α .

Ground-based experiments such as SO- and S4-like

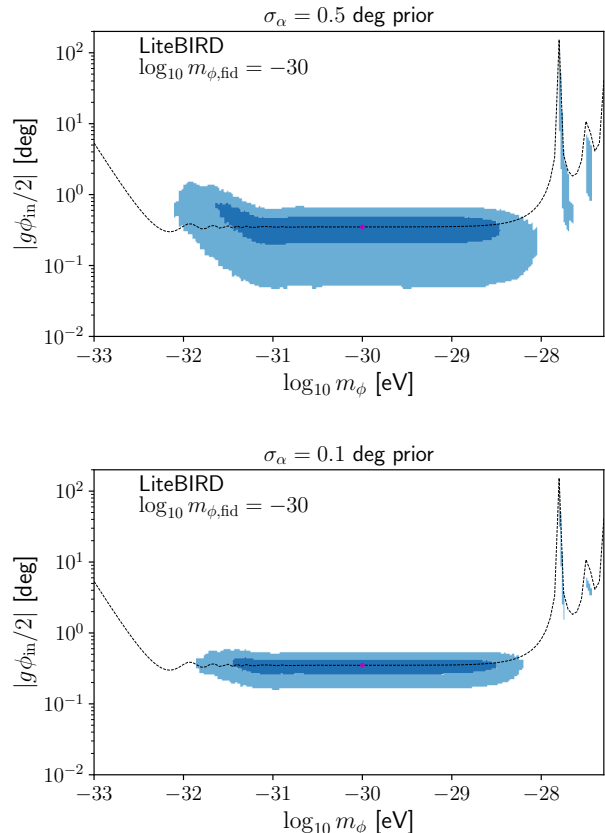


FIG. 9. The expected 1 and 2 σ error contours on $\log_{10} m_\phi$ and $|g\phi_{in}/2|$ (in units of degrees) for $m_{\phi, fid} = 10^{-30}$ eV. The miscalibration angle is marginalized over using a Gaussian prior with $\sigma_\alpha = 0.5$ deg (top) and 0.1 deg (bottom). The fiducial value of $g\phi_{in}/2$ is chosen to give $\beta_{rec} = 0.35$ deg (red dots). The black dashed lines show $|g\phi_{in}/2|$ for $\beta_{rec} = 0.35$ deg at each m_ϕ . We assume a *LiteBIRD*-like experiment.

experiments have better sensitivity to large m_ϕ . In Fig. 11 we show the expected constraints for SO ($m_{\phi, fid} = 10^{-28}$ eV). The constraints tighten significantly compared to the *LiteBIRD*-like case. Some degeneracy between $g\phi_{in}$ and m_ϕ still exist for $\sigma_\alpha = 0.5$ deg (top panel): the shift of peak locations can be absorbed partially by a combination of the rescaled C_l^{EB} and α . The degeneracy is eliminated when a tighter prior is used (bottom panel). With CMB-S4 we can determine m_ϕ precisely, independent of α (see Fig. 12).

As SO and CMB-S4 cannot measure the reionization bump, they can only place an upper bound on m_ϕ if the fiducial mass is 10^{-30} eV. Thus, *LiteBIRD* and ground-based experiments are highly complementary.

V. DISCUSSION

We have made some simplifying assumptions in our calculation of C_l^{EB} . First, we did not include the en-

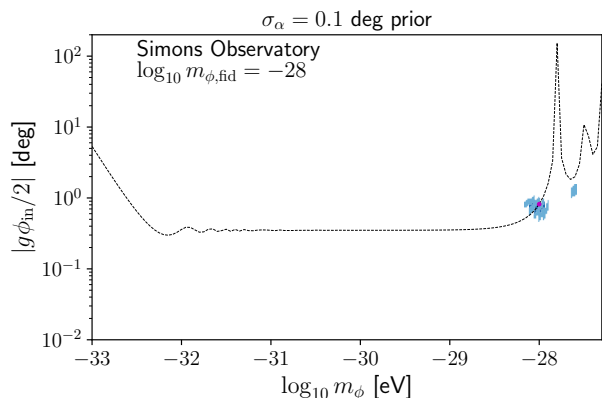
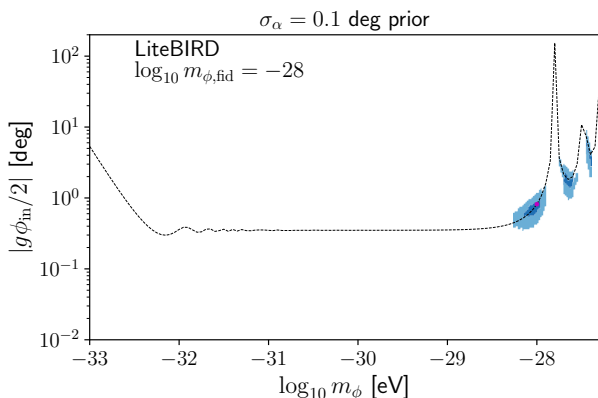
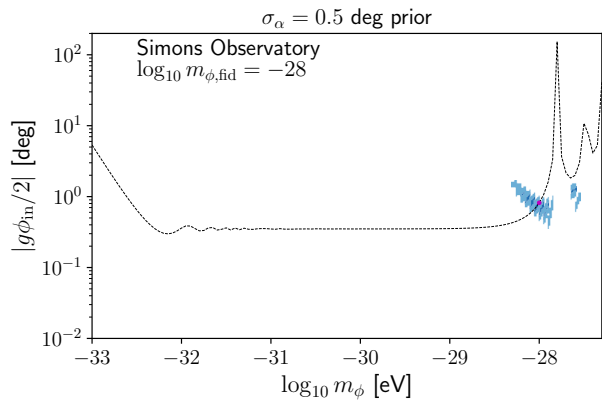
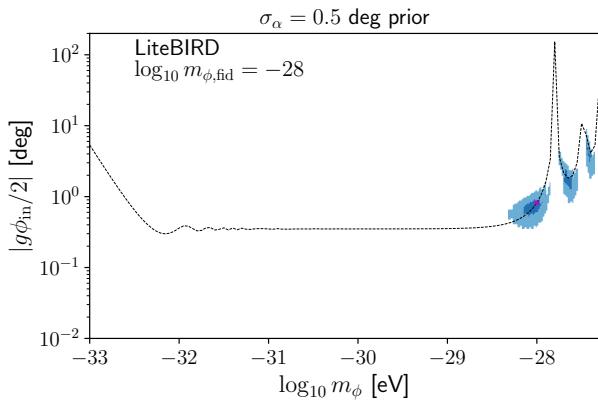


FIG. 10. Same as Fig. 9 but for $m_{\phi, \text{fid}} = 10^{-28}$ eV.

FIG. 11. Same as Fig. 10 but for an SO-like experiment.

ergy density of ϕ in the Friedmann equation explicitly. This assumption can be justified to some extent. For $m_{\phi} \lesssim 10^{-33}$ eV, ϕ acts as dark energy and its energy density is included approximately as a cosmological constant in the Friedmann equation for Λ CDM cosmology. For 10^{-32} eV $\lesssim m_{\phi} \lesssim 10^{-25.5}$ eV, ϕ acts as a small fraction of dark matter today with the density parameter $\Omega_{\phi} h^2 \lesssim 0.006$ [61], which may be ignored for the current study. However, the change in shape of C_l^{EB} at high l is a subtle effect, which can be influenced quantitatively when Ω_{ϕ} is included in the Friedmann equation. We leave the full treatment for future work.

Second, we did not vary cosmological parameters when calculating the expected future constraints on the axion parameters. This assumption can also be justified, as the effect of ϕ on C_l^{EB} is distinct from the cosmological parameter dependence of the parity-even temperature and polarization power spectra. Nevertheless, there may still be some subtle correlation between the cosmological parameters and the axion parameters, which should be accounted for when the axion energy density is included in the Friedmann equation.

We now discuss possible future extensions of the calculation. We did not include inhomogeneity in ϕ , which causes anisotropic polarization rotation [62–64]. While there is no evidence for anisotropic birefringence [65–68],

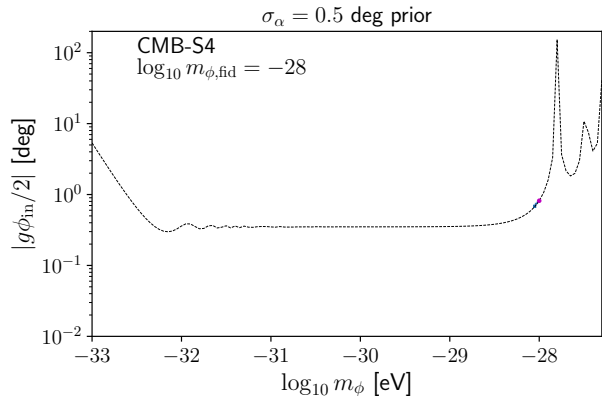


FIG. 12. Same as the top panel of Fig. 11 but for a CMB-S4-like experiment. The result for $\sigma_{\alpha} = 0.1$ deg is similar.

it seems natural to expect discovery of anisotropy if the 3σ hint of isotropic birefringence [16–18] is confirmed with higher statistical significance in future. Thus, incorporating anisotropic birefringence in the Boltzmann equation [35, 48] would be a natural next step.

We ignored the gravitational lensing effect on C_l^{EB} . The lensing would smear the acoustic peaks of C_l^{EB} and

enhance the small-scale power, but these effects would not be degenerate with cosmic birefringence. Nevertheless, for completeness, the impact of the lensing effect will be included in future work.

We have so far focused on cosmic birefringence by a single axion field, but it is entirely possible that cosmic birefringence is induced by multiple fields [15, 69]. In this case, the time evolution of $\beta(\eta)$ becomes more interesting, which can be constrained by the tomographic approach. In this paper we considered two epochs, reionization and recombination, during which the polarization is efficiently generated. Other sources of polarization include the polarized Sunyaev-Zeldovich effect in clusters of galaxies, the so-called remote quadrupole [70–73]. The polarization is generated after the epoch of reionization, and we can in principle use such large-scale polarization signals to probe $\beta(\eta)$ in a late-time Universe.

VI. CONCLUSION

In this paper, we solved the Boltzmann equation coupled with the EoM for an axionlike field ϕ to calculate the detailed shape of the EB power spectrum of the CMB due to cosmic birefringence. There are two critical axion masses: (1) $m_\phi \gtrsim 10^{-32}$ eV, for which relative amplitudes of the reionization bump ($l \lesssim 10$) and the high- l power spectrum are modified; and (2) $m_\phi \gtrsim 10^{-28}$ eV, for which the evolution of ϕ during recombination yields complex features (such as a shift in the locations of acoustic peaks) at high l . Such a change in shape cannot be mimicked fully by the miscalibration angle α , offering a powerful probe of m_ϕ . In Ref. [23], this phenomenon was called “cosmic birefringence tomography,” as it allows us

to measure the time evolution of ϕ .

Probing the first critical mass requires a full-sky coverage by a satellite mission such as *LiteBIRD* [24], whereas the second one can be probed by ground-based experiments [25–27]. The important application of tomography is to distinguish whether ϕ is dark energy or (a fraction of) dark matter today. A convincing detection of the relative amplitude change of the low- and high- l power spectrum by *LiteBIRD* would rule out ϕ being dark energy. Ground-based experiments can constrain the value of m_ϕ , especially at $\gtrsim 10^{-28}$ eV, almost independently of α . Together they can discover new physics and provide new scientific opportunities for CMB experiments [9].

Finally, the EB data at high l from on-going ground-based CMB experiments such as Polarbear [74], Atacama Cosmology Telescope [75], and South Pole Telescope [76] may already set interesting constraints on m_ϕ .

ACKNOWLEDGMENTS

We thank K. Murai, I. Obata, and M. Shiraishi for discussion and comments. This work was supported in part by JSPS KAKENHI Grant No. JP19J21974 (H.N.), No. JP20H05850 (E.K.) and No. JP20H05859 (T.N. and E.K.), Advanced Leading Graduate Course for Photon Science (H.N.), the Deutsche Forschungsgemeinschaft (DFG, German Research Foundation) under Germany’s Excellence Strategy - EXC-2094 - 390783311 (E.K.), and the European Union’s Horizon 2020 research and innovation programme under the Marie Skłodowska-Curie grant agreement No. 101007633 (E.K.). The Kavli IPMU is supported by World Premier International Research Center Initiative (WPI), MEXT, Japan.

-
- [1] D. J. E. Marsh, *Phys. Rept.* **643**, 1 (2016), [arXiv:1510.07633 \[astro-ph.CO\]](#).
 - [2] E. G. M. Ferreira, *Astron. Astrophys. Rev.* **29**, 7 (2021), [arXiv:2005.03254 \[astro-ph.CO\]](#).
 - [3] W.-T. Ni, *Phys. Rev. Lett.* **38**, 301 (1977).
 - [4] M. S. Turner and L. M. Widrow, *Phys. Rev. D* **37**, 2743 (1988).
 - [5] S. M. Carroll, G. B. Field, and R. Jackiw, *Phys. Rev. D* **41**, 1231 (1990).
 - [6] S. M. Carroll and G. B. Field, *Phys. Rev. D* **43**, 3789 (1991).
 - [7] D. Harari and P. Sikivie, *Phys. Lett. B* **289**, 67 (1992).
 - [8] A. Lue, L.-M. Wang, and M. Kamionkowski, *Phys. Rev. Lett.* **83**, 1506 (1999), [arXiv:astro-ph/9812088](#).
 - [9] E. Komatsu, *arXiv e-prints* (2022), [arXiv:2202.13919 \[astro-ph.CO\]](#).
 - [10] S. M. Carroll, *Phys. Rev. Lett.* **81**, 3067 (1998), [arXiv:astro-ph/9806099](#).
 - [11] S. Panda, Y. Sumitomo, and S. P. Trivedi, *Phys. Rev. D* **83**, 083506 (2011), [arXiv:1011.5877 \[hep-th\]](#).
 - [12] F. Finelli and M. Galaverni, *Phys. Rev. D* **79**, 063002 (2009), [0802.4210](#).
 - [13] M. A. Fedderke, P. W. Graham, and S. Rajendran, *Phys. Rev. D* **100**, 015040 (2019), [arXiv:1903.02666 \[astro-ph.CO\]](#).
 - [14] R. C. Myers and M. Pospelov, *Phys. Rev. Lett.* **90**, 211601 (2003), [arXiv:hep-ph/0301124](#).
 - [15] A. Arvanitaki, S. Dimopoulos, S. Dubovsky, N. Kaloper, and J. March-Russell, *Phys. Rev. D* **81**, 123530 (2010), [arXiv:0905.4720 \[hep-th\]](#).
 - [16] Y. Minami and E. Komatsu, *Phys. Rev. Lett.* **125**, 221301 (2020), [arXiv:2011.11254 \[astro-ph.CO\]](#).
 - [17] P. Diego-Palazuelos *et al.*, *Phys. Rev. Lett.* **128**, 091302 (2022), [arXiv:2201.07682 \[astro-ph.CO\]](#).
 - [18] J. R. Eskilt, *arXiv e-prints* (2022), [arXiv:2201.13347 \[astro-ph.CO\]](#).
 - [19] A. Kosowsky, *Annals Phys.* **246**, 49 (1996), [arXiv:astro-ph/9501045](#).
 - [20] M. Zaldarriaga, *Phys. Rev. D* **55**, 1822 (1997), [arXiv:astro-ph/9608050](#).
 - [21] G.-C. Liu, S. Lee, and K.-W. Ng, *Phys. Rev. Lett.* **97**, 161303 (2006), [arXiv:astro-ph/0606248](#).
 - [22] E. Komatsu *et al.* (WMAP), *Astrophys. J. Suppl.* **180**, 330 (2009), [arXiv:0803.0547 \[astro-ph\]](#).

- [23] B. D. Sherwin and T. Namikawa, arXiv e-prints (2021), arXiv:2108.09287 [astro-ph.CO].
- [24] E. Allys *et al.* (LiteBIRD), arXiv e-prints (2022), arXiv:2202.02773 [astro-ph.IM].
- [25] P. Ade *et al.* (Simons Observatory), *J. Cosmol. Astropart. Phys.* **02** (2019), 056, arXiv:1808.07445 [astro-ph.CO].
- [26] L. Moncelsi *et al.*, *Proc. SPIE Int. Soc. Opt. Eng.* **11453**, 1145314 (2020), arXiv:2012.04047 [astro-ph.IM].
- [27] K. N. Abazajian *et al.* (CMB-S4), arXiv e-prints (2016), arXiv:1610.02743 [astro-ph.CO].
- [28] N. J. Miller, M. Shimon, and B. G. Keating, *Phys. Rev. D* **79**, 103002 (2009), arXiv:0903.1116 [astro-ph.CO].
- [29] E. Y. S. Wu *et al.* (QUAD), *Phys. Rev. Lett.* **102**, 161302 (2009), arXiv:0811.0618 [astro-ph].
- [30] E. Komatsu *et al.* (WMAP), *Astrophys. J. Suppl.* **192**, 18 (2011), arXiv:1001.4538 [astro-ph.CO].
- [31] B. G. Keating, M. Shimon, and A. P. S. Yadav, *Astrophys. J. Lett.* **762**, L23 (2012), arXiv:1211.5734 [astro-ph.CO].
- [32] N. Krachmalnicoff *et al.* (LiteBIRD), *J. Cosmol. Astropart. Phys.* **01** (2022), 039, arXiv:2111.09140 [astro-ph.CO].
- [33] Y. Minami, H. Ochi, K. Ichiki, N. Katayama, E. Komatsu, and T. Matsumura, *PTEP* **2019**, 083E02 (2019), arXiv:1904.12440 [astro-ph.CO].
- [34] G. Gubitosi, M. Martinelli, and L. Pagano, *J. Cosmol. Astropart. Phys.* **12** (2014), 020, arXiv:1410.1799 [astro-ph.CO].
- [35] S. Lee, G.-C. Liu, and K.-W. Ng, *The Universe* **4**, 29 (2016), arXiv:1912.12903 [astro-ph.CO].
- [36] H. Cai and Y. Guan, arXiv e-prints (2021), arXiv:2111.14199 [astro-ph.CO].
- [37] T. Fujita, Y. Minami, K. Murai, and H. Nakatsuka, *Phys. Rev. D* **103**, 063508 (2021), arXiv:2008.02473 [astro-ph.CO].
- [38] M. Zaldarriaga and U. Seljak, *Phys. Rev. D* **55**, 1830 (1997), arXiv:astro-ph/9609170.
- [39] M. Kamionkowski, A. Kosowsky, and A. Stebbins, *Phys. Rev. D* **55**, 7368 (1997), arXiv:astro-ph/9611125.
- [40] J. Lesgourgues, arXiv e-prints (2011), arXiv:1104.2932 [astro-ph.IM].
- [41] D. Blas, J. Lesgourgues, and T. Tram, *J. Cosmol. Astropart. Phys.* **07** (2011), 034.
- [42] Planck Collaboration VI, *Astron. Astrophys.* **641**, A6 (2020), [Erratum: *Astron. Astrophys.* 652, C4 (2021)], arXiv:1807.06209 [astro-ph.CO].
- [43] S. Seager, D. D. Sasselov, and D. Scott, *Astrophys. J. Suppl.* **128**, 407 (2000), arXiv:astro-ph/9912182.
- [44] S. Seager, D. D. Sasselov, and D. Scott, *Astrophys. J. Lett.* **523**, L1 (1999), arXiv:astro-ph/9909275.
- [45] W. Y. Wong, A. Moss, and D. Scott, *Mon. Not. Roy. Astron. Soc.* **386**, 1023 (2008), arXiv:0711.1357 [astro-ph].
- [46] A. Lewis, *Phys. Rev. D* **78**, 023002 (2008), arXiv:0804.3865 [astro-ph].
- [47] B. Feng, H. Li, M.-z. Li, and X.-m. Zhang, *Phys. Lett. B* **620**, 27 (2005), arXiv:hep-ph/0406269.
- [48] L. M. Capparelli, R. R. Caldwell, and A. Melchiorri, *Phys. Rev. D* **101**, 123529 (2020), arXiv:1909.04621 [astro-ph.CO].
- [49] M. Tegmark, A. Taylor, and A. Heavens, *Astrophys. J.* **480**, 22 (1997), astro-ph/9603021.
- [50] J. Errard, S. M. Feeney, H. V. Peiris, and A. H. Jaffe, *JCAP* **03** (2016), 052, arXiv:1509.06770 [astro-ph.CO].
- [51] T. Namikawa, *Mon. Not. R. Astron. Soc.* **506**, 1250 (2021), arXiv:2105.03367 [astro-ph.CO].
- [52] T. Namikawa *et al.*, *Phys. Rev. D* **105**, 023511 (2022), arXiv:2110.09730 [astro-ph.CO].
- [53] K. Abazajian *et al.* (CMB-S4), *Astrophys. J.* **926**, 54 (2022), arXiv:2008.12619 [astro-ph.CO].
- [54] Y. D. Takahashi *et al.*, *Astrophys. J.* **711**, 1141 (2010), arXiv:0906.4069 [astro-ph.CO].
- [55] Planck Collaboration Int. XLIX, *Astron. Astrophys.* **596**, A110 (2016), arXiv:1605.08633.
- [56] B. J. Koopman, *Detector Development and Polarization Analyses for the Atacama Cosmology Telescope*, Ph.D. thesis, Cornell U. (2018).
- [57] B. R. Johnson, C. J. Vourch, T. D. Drysdale, A. Kalman, S. Fujikawa, B. Keating, and J. Kaufman, *J. Astron. Inst.* **04**, 1550007 (2015), arXiv:1505.07033 [astro-ph.IM].
- [58] J. P. Kaufman, B. G. Keating, and B. R. Johnson, *Mon. Not. Roy. Astron. Soc.* **455**, 1981 (2016), arXiv:1409.8242 [astro-ph.CO].
- [59] F. Nati, M. J. Devlin, M. Gerbino, B. R. Johnson, B. Keating, L. Pagano, and G. Teply, *J. Astron. Inst.* **06**, 1740008 (2017), arXiv:1704.02704 [astro-ph.IM].
- [60] F. J. Casas, E. Martínez-González, J. Bermejo-Ballesteros, S. García, J. Cubas, P. Vielva, R. B. Barreiro, and A. Sanz, *Sensors* **21**, 3361 (2021).
- [61] R. Hlozek, D. Grin, D. J. E. Marsh, and P. G. Ferreira, *Phys. Rev. D* **91**, 103512 (2015), arXiv:1410.2896 [astro-ph.CO].
- [62] M. Li and X. Zhang, *Phys. Rev. D* **78**, 103516 (2008), arXiv:0810.0403 [astro-ph].
- [63] M. Pospelov, A. Ritz, C. Skordis, A. Ritz, and C. Skordis, *Phys. Rev. Lett.* **103**, 051302 (2009), arXiv:0808.0673 [astro-ph].
- [64] M. Kamionkowski, *Phys. Rev. Lett.* **102**, 111302 (2009), arXiv:0810.1286 [astro-ph].
- [65] D. Contreras, P. Boubel, and D. Scott, *J. Cosmol. Astropart. Phys.* **12** (2017), 046, arXiv:1705.06387 [astro-ph.CO].
- [66] T. Namikawa *et al.*, *Phys. Rev. D* **101**, 083527 (2020), arXiv:2001.10465 [astro-ph.CO].
- [67] F. Bianchini *et al.*, *Phys. Rev. D* **102**, 083504 (2020), arXiv:2006.08061 [astro-ph.CO].
- [68] A. Gruppuso, D. Molinari, P. Natoli, and L. Pagano, *J. Cosmol. Astropart. Phys.* **11** (2020), 066, arXiv:2008.10334 [astro-ph.CO].
- [69] I. Obata, arXiv e-prints (2021), arXiv:2108.02150 [astro-ph.CO].
- [70] M. Kamionkowski and A. Loeb, *Phys. Rev. D* **56**, 4511 (1997), arXiv:astro-ph/9703118.
- [71] J. Portsmouth, *Phys. Rev. D* **70**, 063504 (2004), arXiv:astro-ph/0402173.
- [72] A.-S. Deutsch, E. Dimastrogiovanni, M. C. Johnson, M. Münchmeyer, and A. Terrana, *Phys. Rev. D* **98**, 123501 (2018), arXiv:1707.08129 [astro-ph.CO].
- [73] A.-S. Deutsch, M. C. Johnson, M. Münchmeyer, and A. Terrana, *J. Cosmol. Astropart. Phys.* **04** (2018), 034, arXiv:1705.08907 [astro-ph.CO].
- [74] S. Adachi *et al.* (Polarbear), *Astrophys. J.* **904**, 65 (2020), arXiv:2005.06168 [astro-ph.CO].
- [75] S. K. Choi *et al.* (ACT), *J. Cosmol. Astropart. Phys.* **12** (2020), 045, arXiv:2007.07289 [astro-ph.CO].
- [76] D. Dutcher *et al.* (SPT-3G), *Phys. Rev. D* **104**, 022003 (2021), arXiv:2101.01684 [astro-ph.CO].